Tricritical point of the f-electron antiferromagnet USb_2 driven by high magnetic fields

R. L. Stillwell,[1] I-L. Liu,[2,3,4,5] N. Harrison,[6,7] M. Jaime,[6,7] J. R. Jeffries,[1] and N. P. Butch[4,5]

[1]*Materials Science Division, Lawrence Livermore National Laboratory, Livermore, California 94550, USA*

[2]*Chemical Physics Department, University of Maryland, College Park, Maryland 20742, USA*

[3]*Department of Materials Science and Engineering, University of Maryland, College Park, Maryland 20742-2115, USA*

[4]*NIST Center for Neutron Research, National Institute of Science and Technology, Gaithersburg, Maryland 20899, USA*

[5]*Center for Nanophysics and Advanced Materials, Department of Physics, University of Maryland, College Park, Maryland 20742, USA*

[6]*High Magnetic Field Laboratory, Los Alamos National Laboratory, Los Alamos, New Mexico 87545, USA*

[7]*Materials Physics and Applications Division, Los Alamos National Laboratory, Los Alamos, New Mexico 87545, USA*

(Received 3 October 2016; revised manuscript received 10 December 2016; published 12 January 2017)

In pulsed magnetic fields up to 65 T and at temperatures below the Néel transition, our magnetization and magnetostriction measurements reveal a field-induced metamagneticlike transition that is suggestive of an antiferromagnetic to ferrimagnetic ordering. Our data also suggest a change in the nature of this metamagneticlike transition from second- to first-order-like near a tricritical point at $T_{tc} \sim 145$ K and $H_c \sim 52$ T. At high fields for $H > H_c$ we found a decreased magnetic moment roughly half of the moment determined by neutron powder diffraction. We propose that the decreased moment and lack of saturation at high fields indicate the presence of a field-induced ferrimagnetic state above the tricritical point of the H-T phase diagram for USb_2.

DOI: 10.1103/PhysRevB.95.014414

I. INTRODUCTION

The rich physics of actinide and lanthanide materials provides a diverse palette to explore exotic phenomena driven by the itinerancy or localization of the f electrons [1–3]. Uranium intermetallics in particular span the spectrum of materials properties from magnetism to superconductivity and hidden order to heavy fermions with strongly correlated $5f$ electrons [3–6]. Since these properties are driven by strong electron-electron interactions they are particularly amenable to tuning via the application of pressure, doping, and magnetic fields [7–11]. Within uranium intermetallics, the uranium monopnictides and chalcogenides have garnered a great deal of attention because of their varied magnetic states supported by a simple crystal structure. These compounds variously order antiferromagnetically (UX,X = As,P,Sb), ferromagnetically (UY,Y = S,Se,Te), and ferrimagnetically (UAs, UP), sometimes within the same magnetic field or doping phase diagram. Within the UX and UY families the ordering temperatures can be tuned by varying the pnictogen or chalcogen anion. As a particular example, all of the uranium dipnictides (UX_2) transition from paramagnetic to antiferromagnetic (AFM) [12–14], yet while the Néel temperature T_N can be tuned by changing the pnictogen anion, neither T_N nor the ordered magnetic moments change monotonically with increasing pnictogen radius [15]. Similar lattice tuning effects, in this case via high pressure, revealed that T_N in USb_2 is enhanced as a function of increasing pressure, yet at $P = 9.8$ GPa the AFM state unexpectedly disappears and is replaced by ferromagnetic ordering [9]. Given the success of tuning these compounds with doping and pressure, the question naturally arises as to whether they can also be tuned via the application of magnetic fields.

The use of magnetic fields has historically been limited to a select few of these compounds, since commensurate with their higher ordering temperatures, the critical fields exceed those accessible by common, laboratory-based magnet systems. For those compounds that have been studied with magnetic fields, several of them have shown a field-induced metamagneticlike transition, in which they are driven from one ordered state to another by the application of high magnetic fields [16–19]. Both UBi_2 and USb_2 have been shown to have some amount of hybridization between the f and conduction electrons. This connection between the itinerant f electrons and the local moments is seen by the Fermi surface reconstruction that occurs at the AFM transition. One of the other interesting differences within the UX_2 series is that UBi_2 is the only member that maintains the same Fermi surface structure when crossing from the paramagnetic (PM) phase into the AFM phase [7,20,21]. This is because of a lack of zonefolding due to the fact that the UBi_2 AFM state has a unit cell that is the same as the crystal structure. This difference in Fermi surfaces between UBi_2 and USb_2 is manifested most clearly in the anisotropy of the electrical transport along the c axis (001), where there is a factor of 3 increase in the electrical resistivity upon entering the AFM state in USb_2, whereas there is a negligible increase for UBi_2 [7,22,23]. This effect confirms that the Fermi surface reconstruction that occurs in USb_2 upon entering the AFM phase drives the anisotropic transport properties.

The Fermi surfaces of UBi_2 and USb_2 were measured by Aoki *et al.* deep in the ordered state of both materials ($T \sim 50$ mK). They determined that UBi_2 consists of one spherical Fermi surface at the center of the Brillouin zone and two cylindrical Fermi surfaces at the zone corners [7,20]. In the paramagnetic state UBi_2 and USb_2 share this same Fermi surface structure but as USb_2 transitions into the AFM state the spherical surface at the zone center reconstructs into two cylindrical Fermi surfaces, and hence the high level of anisotropy along the c axis. The effective masses for UBi_2 range from $m^* = 4.4$–$9.2m_0$ (where m_0 is the bare electron mass) and the masses for USb_2 range from $m^* = 2$–$6m_0$. These modestly high masses confirm that there is hybridization between the U $5f$ electrons and the conduction electrons. Taken together with electronic specific heat coefficients of

$\sim 20\,\mathrm{mJ/mol\,K^2}$ and the detection of a narrow dispersing band by angle-resolved photoemission spectroscopy, USb_2 is understood as a partially itinerant antiferromagnet with moderately strong electronic interactions [24,25]. Given the hybridization in USb_2, the anisotropy of the magnetic ordering and high ordering temperature, it seemed reasonable to conclude that high-magnetic fields would be needed to perturb the ground state of this material and investigate the magnetic ordering.

High magnetic fields have proven to be a valuable tool to study many U based intermetallic and heavy fermion compounds because of their ability to reversibly tune and interrogate electronic properties and structure [4,26]. Indeed, hybridization effects in many $5f$ materials, such as UNiAl and UCo_2Si_2, manifest as a field-induced metamagneticlike transition at relatively high magnetic fields, followed by a slow saturation of the magnetic moment, an effect that occurs in fields in excess of 65 T in the case of UCo_2Si_2 [27,28]. With the development of facilities that can routinely reach 65 to 100 T nondestructively, we now have the ability to investigate many of these uranium compounds with ordering temperatures of $T_{N,C} \sim 100-200\,\mathrm{K}$. To that end we have performed magnetostriction and magnetization measurements on USb_2 in high magnetic fields to address whether the AFM transition can be tuned with magnetic field and if there is a structural distortion concomitant with the magnetic transition.

II. EXPERIMENT

Single crystals of USb_2 were grown via self-flux with excess Sb using a U:Sb ratio of 1:6. Depleted U (3N7, New Brunswick Laboratories) and Sb (4N, ESPI Metals) were combined in an alumina crucible, which was sealed in a quartz tube under a partial pressure of UHP Ar. The materials were heated to 1100 °C and held for 96 h, then slow cooled to 800 °C over 100 h, after which the excess flux was spun off in a centrifuge. The crystals formed as platelets up to about 5 mm on a side. Powder and Laue x-ray diffraction were used to confirm the crystal structure and single-crystal nature of the samples.

Magnetostriction and thermal expansion measurements were performed via an optical fiber Bragg grating (FBG) dilatometer [29,30]. Oriented single crystals of USb_2 were attached to a 125 μm diameter telecom-type optical fiber using cyanoacrylate adhesive. The samples were positioned along the length of the fiber where the index of refraction had been modulated so as to reflect a particular wavelength of light known as the Bragg wavelength (λ_B), which would shift due to mechanical compression or expansion of the fiber. In order to increase the signal from the magnetostriction along the c axis, six single crystals (platelets $\sim$0.2 mm thick) were stacked up and glued together to make a stack of $\sim$1 mm total length before attaching them to the fiber (Fig. 1, upper left inset). The reflected light was collected using a monochromator and an InGaAs line-array camera working at 47 kHz. The wavelength of the reflection peak as a function of time $\lambda_B(t)$ is used to compute $\Delta L/L$ on the sample as a function of applied magnetic field. Magnetostriction measurements were made in pulsed magnetic fields up to 65 T at the National High Magnetic Field Laboratory (NHMFL), Los Alamos, with a pulse duration of 25 ms. Sample temperature was controlled using a resistive heater on the probe and thermal connection to the sample in gas was made by attaching a 25 μm gold wire between the sample and the Cernox thermometer using silver epoxy.

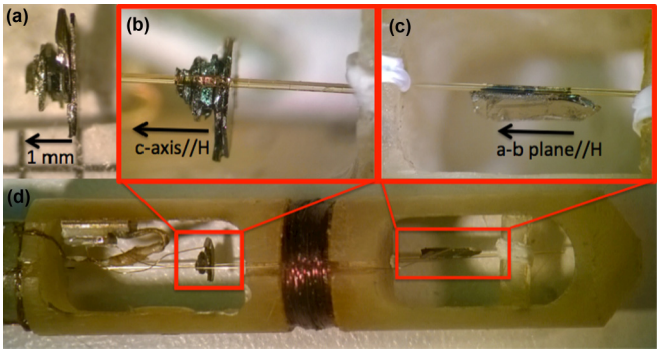

FIG. 1. Experimental setup for the fiber Bragg dilatometer showing the orientations of the USb_2 crystals. The samples shown in (a) were stacked along the c axis to make a total height of 1 mm in order to increase the signal. (b) The stack was glued to the fiber optic cable so that the c axis//H. (c) Crystal of USb_2 glued with the $a-b$ plane of the crystal attached to the fiber. (d) Complete experimental setup showing the c-axis stack (lower left red box), the $a-b$ plane attached along the crystal edge, the position of the thermometer (upper left corner), the magnetic pick-up coil used for magnetic field calibration wrapped around the holder (between the two samples), the gold wires attaching the samples to the thermometer in order to achieve thermal equilibrium.

Magnetization measurements up to 65 T were performed at the NHMFL using an inductively driven, compensated, extraction-coil magnetometer [31]. In addition to the compensated coils, electronic balancing was also used in order to compensate for any nonuniform thermal contraction of the coils during cooling. A $50 \times 50 \times 100\,\mu$m rectangular sample was mounted in a PTFE capsule using Apiezon N grease with the [001] axis oriented along the applied magnetic field direction. The capsule was then mounted on a long, thin rod reaching from the sample capsule to the top of the probe that could extract the sample out of the coil in order to perform field sweeps of the empty coil for background subtraction. Additional magnetization measurements up to 15 T were performed using the Vibrating Sample Magnetometer option of a Quantum Design Physical Properties Measurement System [32] in order to calibrate the high field data collected at the NHMFL.

III. RESULTS AND DISCUSSION

A. Thermal expansion and magnetostriction

Initial thermal expansion measurements were made in zero magnetic field where the AFM transition was visible as a second-order transition in $\Delta L/L$ versus temperature, and is clearly seen in the coefficient of the thermal expansion $d\Delta L/L/dT$ or $\alpha(T)$, at $T_N = 202.3\,\mathrm{K}$ (bottom inset of Fig. 2), which matches with previously reported values [7,15,23,33]. The USb_2 crystals form as platelets in the $a-b$ plane, with the thinner layers forming along the c axis. The thermal expansion data shown in Fig. 2 was acquired with the platelet oriented

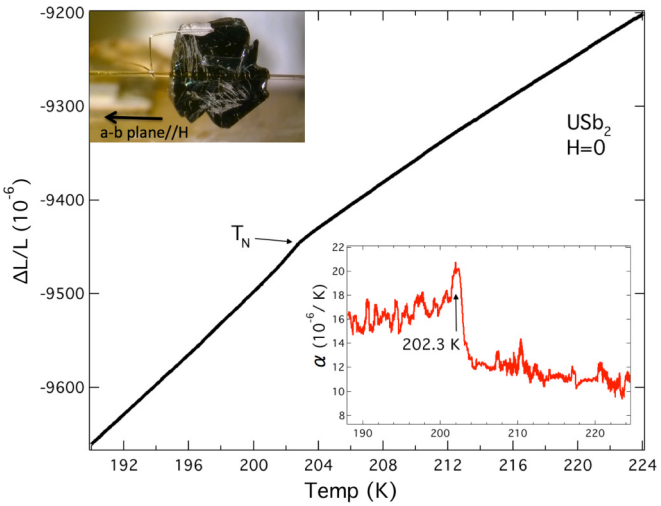

FIG. 2. Thermal contraction as a function of temperature during cooling of USb_2 along the $a-b$ plane. A picture of the samples attached to the fiber Bragg grating oriented with H along the $a-b$ plane (shown in the top, right inset), and the stack of six crystals attached to the FBG with H along the c axis (shown in the top, left inset). The coefficient of thermal contraction (α, defined as the derivative of $\Delta L/L$ with respect to the temperature) during cooldown (lower inset) is shown to emphasize the location of the AFM transition at $T_N = 202.58$ K, as previously reported in the literature.

with the $a-b$ plane along the fiber/magnetic field (Fig. 1 upper inset). Magnetostriction experiments were performed on crystals oriented both with H along the $a-b$ plane and along the c axis. The plot of $\Delta L/L$ versus applied magnetic field with the field along the easy axis c shows a field-induced phase transition for $T < T_N$ (Fig. 3). The transition continues to move to higher applied fields as the temperature is lowered reaching $H_c = 63$ T at $T = 80$ K (Fig. 4). The magnetostriction for H

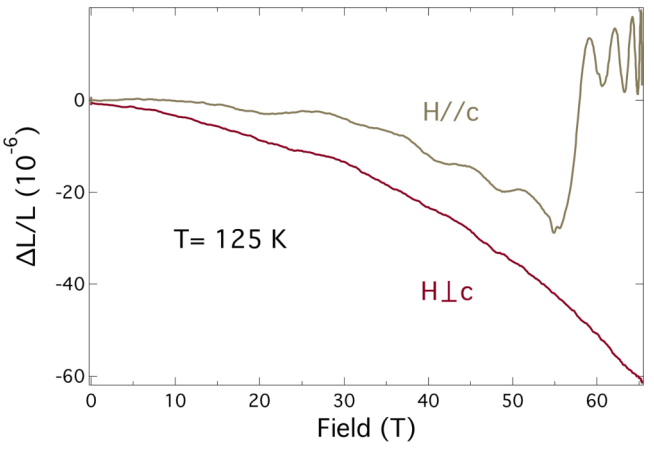

FIG. 3. Comparison of the magnetostriction as a function of applied magnetic field, for $H//c$ axis and H perpendicular to the c axis at $T = 125$ K. The anisotropy of the system is clearly demonstrated by the metamagneticlike transition seen for $H//c$ axis, but not with H perpendicular to c axis. All of the $\Delta L/L$ data shown in the following figures is for $H//c$ axis. Oscillations for $H//c$ are likely due to vibrations resulting from the small misalignment of magnetic moment with the applied magnetic field.

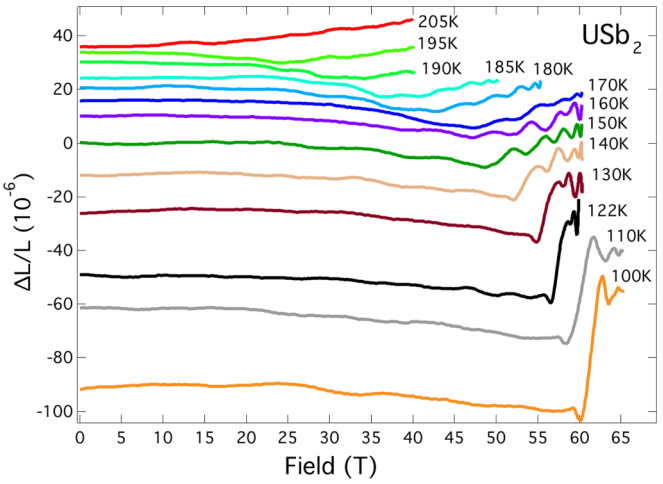

FIG. 4. $\Delta L/L$ as a function of applied magnetic field, measured with the $H//c$ axis. Measurements at temperatures above and below the AFM transition are shown. For $T > T_N$ there is no evidence of a transition, but for $T < T_N$ there is a change in slope that grows increasingly sharp as the temperature is decreased, with a second-order-like to first-order-like tricritical point at $T_{tc} \sim 145$ K. There is also a change in the slope of the $\Delta L/L$ for $H > H_c$ and $T < 140$ K. All traces are offset vertically for clarity.

along the $a-b$ plane did not show the field-induced phase transition for any temperatures $T < T_N$ up to 65 T, confirming that the magnetic hard axis is in the $a-b$ plane and that there is a strong anisotropy between the c axis and the $a-b$ plane in USb_2.

Interestingly, as the temperature is lowered the phase transition goes from second-order-like to first-order-like near $T = 150$ K. This can be seen clearly in Fig. 4, where the transition becomes nearly discontinuous for $T \leqslant 122$ K. In addition to the crossover to first-order-like, the amplitude of the transition also increases as the temperature is lowered [Figs. 4 and 5(a)]. We determined the amplitude of the transition by fitting a straight line to the data for 10 T before the transition and another straight line to the data for $H > H_c$, and then found the amplitude of the change between these two lines [see Fig. 10]. This change in the lattice at the field-induced phase transition demonstrates that there is a strong magnetoelastic effect. The magnetoelastic coupling in USb_2 shown in our data is also seen in many other 5 f-electron systems, including the uranium monochalcogenides, $UCu_{0.95}Ge$, and UPt_2Si_2 [8,18,34]. This magnetoelastic transition could indicate a structural phase transition accompanying the magnetic phase transition, similar to the cubic rock salt to rhombohedral distortion in uranium sulfide as it enters the ferromagnetic state [35–38].

B. Magnetization

In order to further investigate the magnetoelastic transition we also performed magnetization measurements on a single crystal of USb_2 above and below the Néel transition. We clearly observed the field-induced metamagneticlike transition for $T < T_N$ (Fig. 6), confirming our magnetostriction measurements. The critical field for the transition increases with decreasing temperature, down to the lowest temperatures and

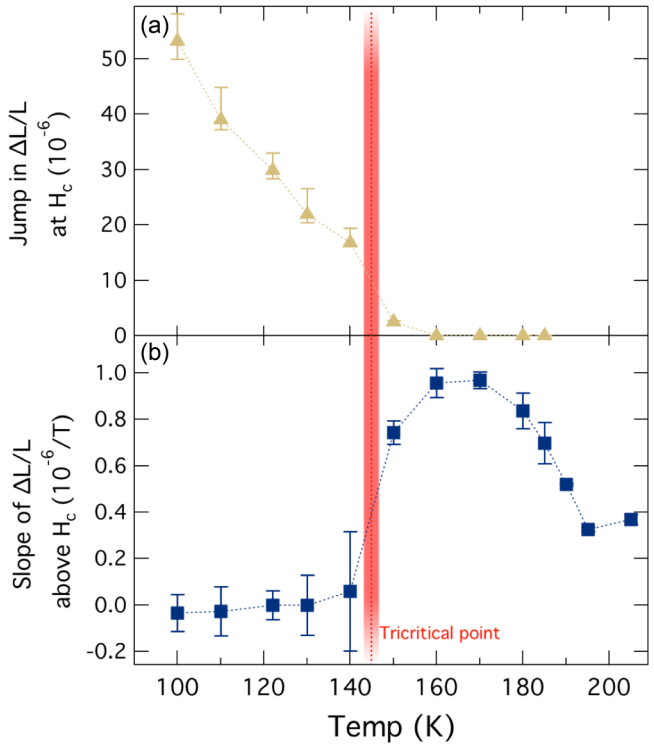

FIG. 5. (a) Amplitude of the jump in $\Delta L/L$ at H_c as a function of temperature. The red stripe at $T = 145$ K is the tricritical temperature as predicted by our calculations. This data show that there is a discontinuous jump in $\Delta L/L$ for $T \leqslant 150$ K and that the amplitude of the jump at H_c increases with decreasing temperature. (b) Plot of the slope of the $\Delta L/L$ above the transition ($H > H_c$) as a function of applied magnetic field. The slope of the $\Delta L/L$ at high temperatures increases initially with decreasing temperature and then decreases. For $T \leqslant 140$ K the slope is nearly zero, within error, which we propose as evidence of a ferrimagnetic state. Error bars for both plots are based on the cumulative variation due to transition width and noise in the data before and after the transition.

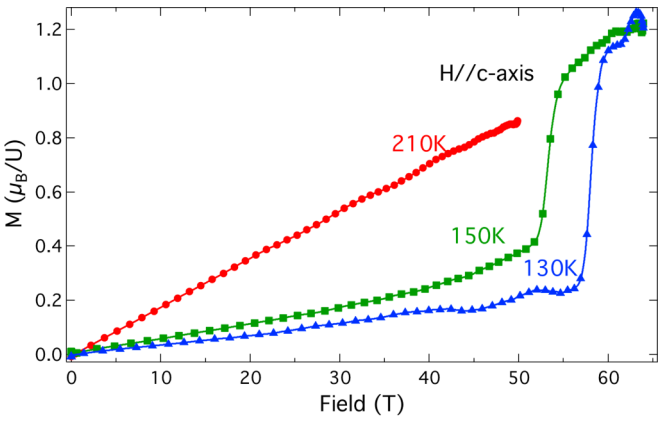

FIG. 6. Magnetization as a function of applied magnetic field for $H//c$ in units of μ_B per uranium atom for selected temperatures. For $T > T_N$ there is a linear trend of the magnetization but for $T < T_N$ there is a metamagneticlike transition. The increase of the magnetization at H_c is roughly $1\,\mu_B$/U, which is nearly a factor of 2 less than the previously measured zero-field moment of $1.88\,\mu_B$/U [33,51]. High-field data was calibrated using a Quantum Design Vibrating Sample Magnetometer up to 15 T.

highest fields studied in this experiment. The critical field for the transition is defined as the intersection point of two straight lines, one fit to the nearly vertical part of the data trace and the other fit to the lower field side of the trace leading up to the nearly vertical section [see Fig. 11]. Error bars for the transition were calculated as the points at which the data trace deviated from the fit lines above and below the transition. There is very good agreement on H_c from both the magnetization and the magnetostriction measurements.

Surprisingly, the change of the magnetization at the transition is only $\Delta M \sim 1\mu_B$, roughly half of the expected moment of $1.88\mu_B$/U found by neutron powder diffraction [33,39]. We propose that this decreased moment is a result of a field-induced ferrimagnetic transition. The increase of $1/2$ of the magnetic moment could be accomplished by one out of every two down (up) spins becoming an up (down) spin. Since USb_2 starts out in the antiferromagnetic-IA $(++--)$ state the ferrimagnetic state would therefore correspond to a $+\,+\,-+$ state. Based on similar systems such as UPd_2Si_2, one could expect to then reach the polarized (or saturated) paramagnetic state with $M = 1.88\mu_B$/U at some higher field than the 65 T achievable in the magnet system used in our experiment [40].

Considering that these are bulk measurements, our statement that the ferrimagnetic state being $+\,+\,-+$ should be understood as a qualitative statement that would achieve an average moment of $1/2$ of the saturation moment, based on the bulk magnetic moment, and not a statement of the actual microscopic arrangement of spins. To truly know the structure would require a microscopic probe of the magnetic structure such as neutron diffraction, which is not possible at these high-magnetic fields at this time, though this may be a possibility in the not-too-distant future, see for instance Ref. [41]. Ferrimagnetic ordering in USb_2 could also be achieved via other spin arrangements using a construction similar to the "blocks of planes" used in Ref. [42] that would have blocks of $+\,+\,-+$ and $+\,+\,--$, or some similar arrangement that would give an equivalent magnetic moment.

Another consistent trend in the two measurements is that the high-field transition grows increasingly sharp as the temperature is decreased. Indeed, the order of the transition seen in magnetization goes from second- to first-order-like near $T = 150$ K and $H = 50$ T, similar to our magnetostriction measurements. The $M(H)$ curves for $155 < T < 180$ K shown in Fig. 7 demonstrate that there is an initial upturn in the magnetization (H^*) before the metamagneticlike transition (H_c), whereas for $T < 155$ K there is no significant increase in magnetization preceding the transition, making the high-field transitions in this region more first-order-like. To further investigate the connection between the metamagneticlike transition and the tricritical point we plot the change in the transition widths of both H^* and H_c as a function of temperature (Fig. 8). There is a clear onset of the H^* transition width for $T > T_{tc}$ that can be seen in both Figs. 7 and 8(a). The transition width of the metamagneticlike transition at H_c also changes near the tricritical point, but it is harder to define the endpoints since the transition is not as sharp at higher temperatures. Taken together, the magnetostriction and magnetization as a function of magnetic field, and the transition widths as a function of temperature, give strong evidence for the presence of a tricritical point near $T = 145$ K

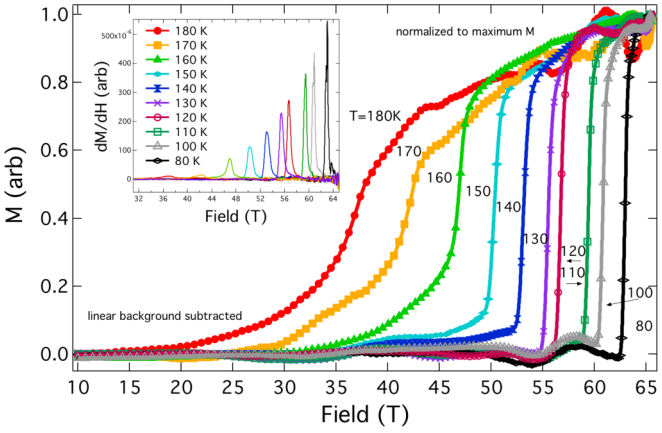

FIG. 7. Plot of magnetization as a function of applied magnetic field for various temperatures. All of the traces were fit with a straight line from zero up to H^*, where the slope of the trace deviates from linearity. All of the traces were then normalized so that the maximum value of the magnetization was equal to one. The upper inset of the figure shows the derivative of the magnetization as a function of magnetic field dM/dH. The change from second to first order can be seen as the lower field side of the derivative becomes discontinuous for $T < 150$ K.

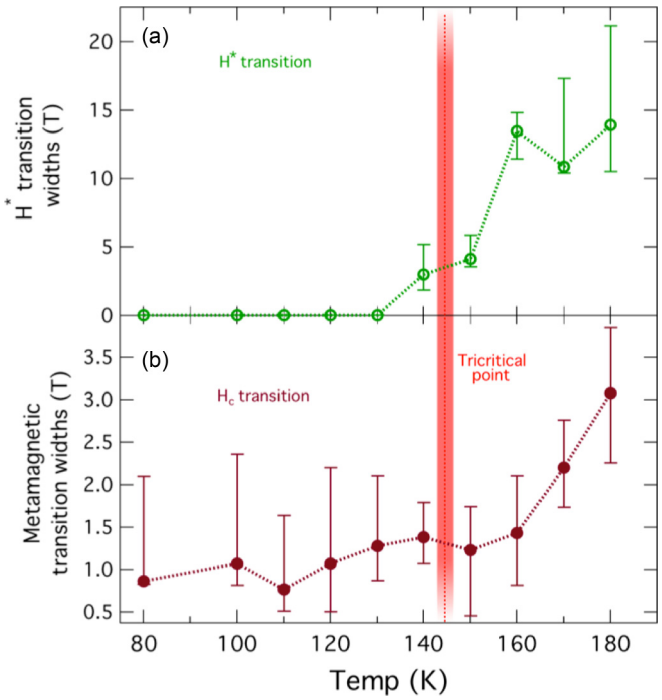

FIG. 8. (a) Width of the second-order-like transition (H^*) in the magnetization as a function of temperature. The width of the H^* transition is clearly connected to the tricritical point at 145 K, as the width of the transition goes to zero by 130 K. (b) Plot of the width of the metamagneticlike transition H_c as a function of temperature. The H_c transition width is not as strongly correlated as H^* is to the order of the transition, nonetheless the trend of the data shows a decrease of the transition width as the temperature approaches $T \sim T_{tc}$. The error bars represent the variation allowed by different straight-line fits to the data.

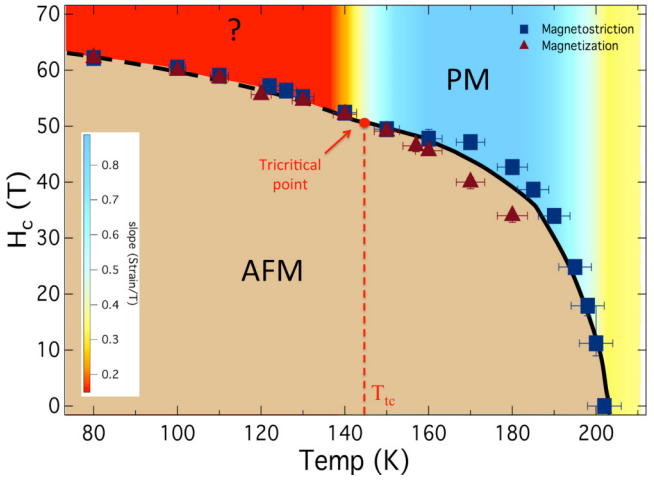

FIG. 9. Magnetic field and temperature phase diagram of USb_2 ($T_N = 202.3$ K), compiled from both magnetostriction and magnetization data. The predicted tricritical point is shown at $T_{tc} = 145$ K, with the red dashed line intersecting the phase boundary at $H = 52$ T. The phase boundary is drawn with a solid black line for $T > 145$ K to indicate that the metamagneticlike transition is second-order-like, whereas it is drawn as a dashed line for $T < 145$ K where the metamagneticlike transition is first-order-like. The intensity plot above the phase boundary shows the slope of the $\Delta L/L$ versus magnetic field above the metamagneticlike transition ($H > H_c$).

and $H = 52$ T. This second- to first-order-like transition is illustrated in the phase diagram in Fig. 9 by using a solid line along the phase boundary to represent the second-order-like transitions and a dashed line along the phase boundary to represent the first-order-like transitions.

This second- to first-order-like tricritical point is similar to that seen in canonical metamagnets such as $FeCl_2$, $CoCl_2$, and $Ni(NO_3)_2 \cdot H_2O$ and more recently in $CeRh_2Si_2$ and other $(U,Ce)X_2Si_2$ systems [43–47]. Following the work of Bidaux *et al.* [48] we calculated the tricritical temperature using the mean-field formula for a two sublattice antiferromagnet with ferromagnetic intralayer coupling such that

$$T_{tc} = \frac{2}{3}\frac{T_N(T_N + 2\theta)}{T_N + \theta},$$

where T_{tc} is the tricritical point where the transition goes from second- to first-order-like, T_N is the Néel temperature, and θ is the Weiss constant, found from the slope of $1/\chi$ vs T. Substituting $T_N = 202$ K and $\theta = +18$ K [33] into the equation above we calculate a tricritical temperature $T_{tc} = 145$ K, which corresponds to the temperature at which there is a change in transition amplitude for magnetostriction versus magnetic field [Fig. 5(a)].

To further characterize the high-field magnetic state for $H > H_c$, we also analyzed the slope of the $\Delta L/L$ versus magnetic field, shown in Fig. 5(b) and as an intensity plot in the high-field region of the phase diagram (Fig. 9). To determine the slope, we fit a straight line to all of the $\Delta L/L$ data for $H > H_c$ and then compared the slopes as a function of temperature, with the slope of the line represented by the color scale in Fig. 9 (see inset for scale values). The plot of the slope as a function of temperature in both Figs. 5(b) and 9

demonstrates that there is variation in slope above T_{tc}, but it then decreases and remains nearly zero for all $T < T_{tc}$. The saturation of the slope for $T < T_{tc}$ gives more evidence for a field-induced metamagneticlike transition from the AFM state into a ferrimagnetic state. Although this AFM to ferrimagnetic transition is similar to other UX and UTX systems, it is not possible to definitively claim what the order of the high field state is, since we are limited to the small field range available above the transition as well as the noise in the data in that region [5,16,17,49,50].

IV. CONCLUSIONS

Using high magnetic fields up to 65 T we were able to see a field-induced metamagneticlike transition in both magnetostriction and magnetization measurements enabling us to construct a H-T phase diagram for USb_2. We also observed that the order of the transition changes from second-order-like to first-order-like near a calculated tricritical point at $T_{tc} \sim 145$ K and $H_{tc} \sim 52$ T. By studying the slope of the magnetostriction above H_c we were able to show evidence of a high field state suggestive of ferrimagnetic order, where one out of every two down (up) spins becomes an up (down) spin. The combination of magnetic anisotropy and field-tuned magnetoelastic coupling suggest that future measurements using x-ray or neutron scattering at high field may yield important insight into details of the magnetic structure.

ACKNOWLEDGMENTS

The authors would like to thank Gerry Lander for fruitful discussions. This work was performed under LDRD (Tracking Code 14-ERD-041) and under the auspices of the US Department of Energy by Lawrence Livermore National Laboratory (LLNL) under Contract No. DE-AC52- 07NA27344. A portion of this work was performed at the National High Magnetic Field Laboratory, which is supported by National Science Foundation Cooperative Agreement No. DMR-1157490, the State of Florida, the U.S. Department of Energy and the U.S. office of Science project "Science at 100 T".

APPENDIX

In order to better understand how the transitions in magnetostriction and magnetization were chosen and how the errors were calculated, we have plotted traces from each data set that are representative of a second-order-like and a first-order-like transition. Due to the second-order-like to first-order-like transition this was not a straightforward analysis, especially near the tricritical point.

Figure 10 shows three different traces of magnetostriction as a function of magnetic field. The three different temperatures (180, 140, and 100 K) were chosen to show the range of fitting considerations at temperatures much greater than the tricritical temperature (T_{tc}), very close to T_{tc}, and much less than T_{tc}. Error bars represent the maximum and minimum value that could have been chosen by incorporating: (1) variation due to the noise in the high-field range of the data and (2) variation due to the curvature of the trace before the transition.

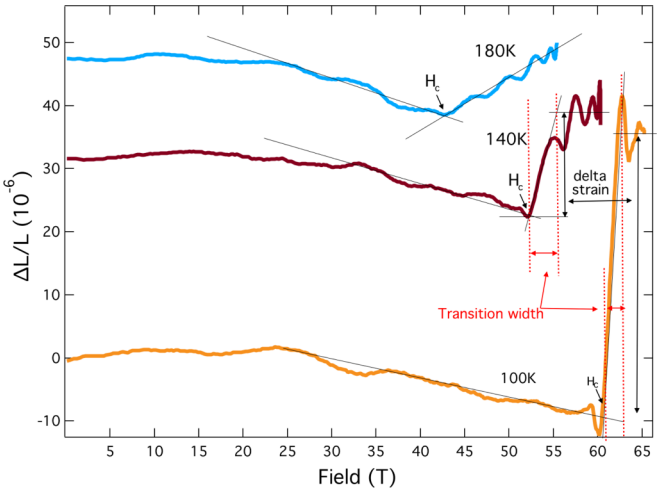

FIG. 10. Magnetostriction as a function of applied magnetic field for three temperatures showing how H_c, transition width, and the change in strain at the transition were measured. H_c is defined as the intersection point of two straight lines, one on the nearly vertical part of the trace and one on the part of the trace before going nearly vertical. Error bars represent the maximum and minimum value that could have been chosen by incorporating the curvature of the trace before the transition and the noise in the trace above the transition into the straight-line fits to the data.

Figure 11 shows two magnetization traces, one at 160 K where the transition is still second-order-like, and another trace at 80 K where the transition is first-order-like. The low field part of the curve was fit with a straight line, as was the curve above the transition. H^* was chosen as the point where there was a clear deviation of the magnetization curve away from the straight-line fit, indicated by the vertical dashed red line

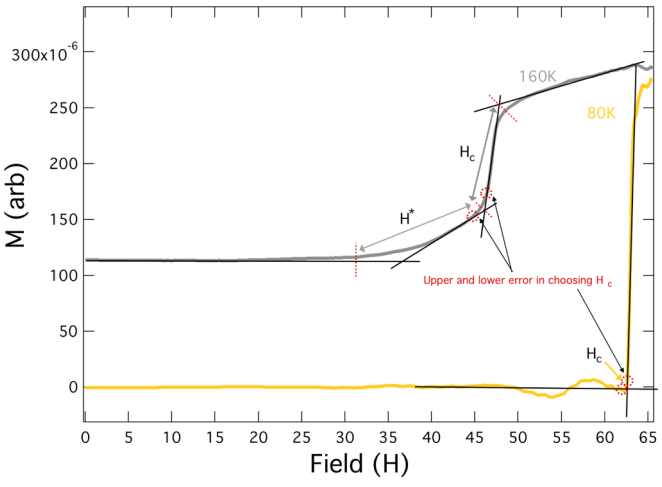

FIG. 11. Magnetization as a function of applied magnetic field for two temperatures showing how H_c, H^*, and the related error bars were chosen. H_c is defined as the intersection point of two straight lines, one on the nearly vertical part of the trace and one on the part of the trace before going nearly vertical. The error is taken as the points where the trace deviates from the straight line. H^* is taken as the point where there is a clear deviation of the magnetization curve from the straight-line fit.

in the low-field side of the curve. The lower error in H^* was taken as the point where the straight-line fit was no longer on top of the magnetization curve. The upper error in H^* was taken as the point where the two straight-line fits intersect. The transition width of H^* is taken as the field range between the lower red, dashed straight line and H_c. The transition width of H_c is taken as the field range between the red, dashed straight line at H_c and the uppermost red, dashed straight line. The errors for the H^* transition width is taken from the upper and lower errors for both transitions. The errors for the H_c transition are taken from the transition error on the low-field side and the points where the magnetization curve deviates from the straight-line fits on the high-field side of the curve.

[1] K.T. Moore and G. van der Laan, Nature of the 5f states in actinide metals, Rev. Mod. Phys. **81**, 235 (2009).

[2] G. R. Stewart, Heavy-fermion systems, Rev. Mod. Phys. **56**, 755 (1984).

[3] A. J. Freeman and J. B. Darby, *The Actinides: Electronic Structure and Related Properties* (Elsevier Science, New York, 2013).

[4] J. A. Mydosh and P. M. Oppeneer, *Colloquium*: Hidden order, superconductivity, and magnetism: The unsolved case of URu_2Si_2, Rev. Mod. Phys. **83**, 1301 (2011).

[5] A. Gourgout, A. Pourret, G. Knebel, D. Aoki, G. Seyfarth, and J. Flouquet, Collapse of Ferromagnetism and Fermi Surface Instability Near Reentrant Superconductivity of URhGe, Phys. Rev. Lett. **117**, 046401 (2016).

[6] H. Abe, H. Suzuki, H. Kitazawa, T. Matsumo, and G. Kido, Successive field induced magnetic phase transitions of heavy fermion compound $CeRh_2Si_2$, J. Phys. Soc. Jpn. **66**, 2525 (1997).

[7] D. Aoki, P. Wiśniewski, K. Miyake, N. Watanabe, Y. Inada, R. Settai, E. Yamamoto, Y. Haga, and Y. Onuki, Cylindrical Fermi surfaces formed by a flat magnetic Brillouin zone in uranium dipnictides, Philos. Mag. B **80**, 1517 (2000).

[8] D. Schulze Grachtrup, M. Bleckmann, B. Willenberg, S. Süllow, M. Bartkowiak, Y. Skourski, H. Rakoto, I. Sheikin, and J. A. Mydosh, Field-induced phases in UPt_2Si_2, Phys. Rev. B **85**, 054410 (2012).

[9] J. R. Jeffries, R. L. Stillwell, S. T. Weir, Y. K. Vohra, and N. P. Butch, Emergent ferromagnetism and T-linear scattering in USb_2 at high pressure, Phys. Rev. B **93**, 184406 (2016).

[10] Z. Henkie, P. Wiśniewski, R. Fabrowski, and R. Maślanka, Dependence of ordering temperature on pressure, carrier density and U-U distance in uranium pnictides; pressure and hall effects examinations of UP_2 and USb_2, Solid State Commun. **79**, 1025 (1991).

[11] N. P. Butch, S. Ran, I. Jeon, N. Kanchanavatee, K. Huang, A. Breindel, M. B. Maple, R. L. Stillwell, Y. Zhao, L. Harriger, and J.W. Lynn, Distinct magnetic spectra in the hidden order and antiferromagnetic phases in $URu_{(2-x)}Fe_xSi_2$, Phys. Rev. B **94**, 201102 (2016).

[12] W. Trzebiatowski, A. Sepichowska, and A. Zygmunt, Magnetic properties of uranium compounds with arsenic or antimony, Bull. Acad. Polonaise Sci. Ser. Sci. Chim. **12**, 687 (1964).

[13] W. Trzebiatowski and R. Troc, Magnetic properties of uranium phosphides, Bull. Acad. Polonaise Sci. Ser. Sci. Chim. **11**, 661 (1963).

[14] W. Trzebiatoski and A. Zygmunt, Magnetic properties of uranium bismuthides, Bull. Acad. Polonaise Sci. Ser. Sci. Chim. **14**, 495 (1966).

[15] G. Amoretti, A. Blaise, and J. Mulak, Crystal-field interpretation of the magnetic-properties of UP_2,UAS_2, USb_2, UBi_2 compounds, J. Magn. Magn. Mater. **42**, 65 (1984).

[16] O. Vogt, P. Wachter, and H. Bartholin, High field magnetization measurements on UP single crystals, Physica B+C **102**, 226 (1980).

[17] G. P. Felcher, G. H. Lander, P. de V. du Plessis, and O. Vogt, Neutron diffraction study of UAs in high magnetic fields, Solid State Commun. **32**, 1181 (1979).

[18] F. A. Wedgewood and M. Kuzneitz, Actinide pnictides and chalcogenides. I. Study of magnetic ordering and ordered moments in uranium monochalcogenides by neutron diffraction, J. Phys. C **5**, 3012 (1972).

[19] G. Busch and O. Vogt, Magnetic anisotropy of single crystals of rocksalt-type uranium compounds, J. Less Common Metals **62**, 335 (1978).

[20] D. Aoki, P. Wiśniewski, K. Miyake, N. Watanabe, Y. Inada, R. Settai, E. Yamamoto, Y. Haga, and Y. Ōnuki, Crystal growth and cylindrical Fermi surfaces of USb_2, J. Phys. Soc. Jpn. **68**, 2182 (1999).

[21] P. Wisniewski, D. Aoki, N. Watanabe, K. Miyake, R. Settai, Y. Onuki, Y. Haga, E. Yamamoto, and Z. Henkie, Shubnikov-de Haas effect study of cylindrical Fermi surfaces in UAs_2, J. Phys.: Condens. Matter **12**, 1971 (2000).

[22] Z. Henkie, R. Maślanka, P. Wiśniewski, R. Fabrowski, P. J. Markowski, J. J. M. Franse, and M. van Sprang, Anisotropy of the physical properties of uniaxial antiferromagnetic USb_2, J. Alloys Compounds **181**, 267 (1992).

[23] R. Wawryk, Magnetic and transport properties of UBi_2 and USb_2 single crystals, Philos. Mag. **86**, 1775 (2006).

[24] A. Blaise, J. M. Fournier, R. Schenkel, M. J. Mortimer, Z. Henkie, and A. Wojakowski, Physical properties of uranium dipnictides, rare earths and actinides, *Conference on rare earths and actinides*, Durham, U.K., 4–6 July, 1977, pp. 184–189.

[25] E. Guziewicz, T. Durakiewicz, M. T. Butterfield, C. G. Olson, J. J. Joyce, A. J. Arko, J. L. Sarrao, D. P. Moore, and L. Morales, Angle-resolved photoemission study of USb_2: The 5f band structure, Phys. Rev. B **69**, 045102 (2004).

[26] D. I. Gorbunov, M. S. Henriques, A. V. Andreev, Y. Skourski, M. Richter, L. Havela, and J. Wosnitza, First-order magnetization process as a tool of magnetic-anisotropy determination: Application to the uranium-based intermetallic $U_3Cu_4Ge_4$, Phys. Rev. B **93**, 064417 (2016).

[27] E. Brück, H. Nakotte, F. R. de Boer, P. F. de Châtel, H. P. van der Meulen, J. J. M. Franse, A. A. Menovsky, N. H. Kim-Ngan, L. Havela, V. Sechovsky, J. A. A. J. Perenboom, N. C. Tuan, and J. Sebek, Electronic properties of UNiAl in high magnetic fields, Phys. Rev. B **49**, 8852 (1994).

[28] A. V. Andreev, S. Yasin, Y. Skourski, A. A. Zvyagin, S. Zherlitsyn, and J. Wosnitza, Magnetic and magnetoelastic properties of UCo_2Si_2 as studied by high-field magnetization and ultrasound measurements, Phys. Rev. B **87**, 214409 (2013).

[29] R. Daou, F. Weickert, M. Nicklas, F. Steglich, A. Haase, and M. Doerr, High resolution magnetostriction measurements in pulsed magnetic fields using fiber Bragg gratings, Rev. Sci. Instrum. **81**, 5 (2010).

[30] M. Jaime, R. Daou, S. A. Crooker, F. Weickert, A. Uchida, A. E. Feiguin, C. D. Batista, H. A. Dabkowska, and B. D. Gaulin, Magnetostriction and magnetic texture to 100.75 Tesla in frustrated $SrCu_2(BO_3)_{(2)}$, Proc. Natl. Acad. Sci. USA **109**, 12404 (2012).

[31] J. A. Detwiler, G. M. Schmiedeshoff, N. Harrison, A. H. Lacerda, J. C. Cooley, and J. L. Smith, Magnetization of UBe_{13} to 60 T, Phys. Rev. B **61**, 402 (2000).

[32] Any mention of commercial products does not imply recommendation or endorsement by NIST.

[33] J. Leciejewicz, R. Troć, A. Murasik, and A. Zygmunt, Neutron-diffraction study of antiferromagnetism in USb_2 and UBi_2, Phys. Status Solidi (b) **22**, 517 (1967).

[34] S. Zherlitsyn, S. Yasin, J. Wosnitza, A. A. Zvyagin, A. V. Andreev, and V. Tsurkan, Spin-lattice effects in selected antiferromagnetic materials (Review Article), Low Temp. Phys. **40**, 123 (2014).

[35] W. J. L. Buyers, T. M. Holden, J. A. Jackman, A. F. Murray, P. de V. DuPlessis, and O. Vogt, Exploration of magnetic excitation behaviour of actinide compounds with neutron scattering, J. Magn. Magn. Mater. **31**, 229 (1983).

[36] J. R. Jeffries, P. Söderlind, H. Cynn, A. Landa, W. J. Evans, S. T. Weir, Y. K. Vohra, and G. H. Lander, Magnetism and structural distortions in uranium sulfide under pressure, Phys. Rev. B **87**, 214104 (2013).

[37] H. Kuwahara, Y. Tomioka, A. Asamitsu, Y. Moritomo, and Y. Tokura, A first-order phase transition induced by a magnetic field, Science **270**, 961 (1995).

[38] Z. W. Ouyang, H. Nojiri, S. Yoshii, G. H. Rao, Y. C. Wang, V. K. Pecharsky, and K. A. Gschneidner, Field-induced magnetostructural transition in Gd_5Ge_4 studied by pulsed magnetic fields, Phys. Rev. B **77**, 184426 (2008).

[39] J. Leciejewicz, Erratum, Phys. Status Solidi **24**, 763 (1967).

[40] T. Honma, H. Amitsuka, S. Yasunami, K. Tenya, T. Sakakibara, H. Mitamura, T. Goto, G. Kido, S. Kawarazaki, Y. Miyako, K. Sugiyama, and M. Date, Incommensurate-commensurate magnetic phase transitions of the Ising-5f system UPd_2Si_2: The $H-T$ phase diagram and mean-field analyses, J. Phys. Soc. Jpn. **67**, 1017 (1998).

[41] Z. Islam, D. Capatina, J. P. C. Ruff, R. K. Das, E. Trakhtenberg, H. Nojiri, Y. Narumi, U. Welp, and P. C. Canfield, A single-solenoid pulsed-magnet system for single-crystal scattering studies, Rev. Sci. Instrum. **83**, 035101 (2012).

[42] J. Rossat-Mignod, G. H. Lander, and P. Burlet, in *Handbook on the Physics and Chemistry of the Actinides*, edited by A. J. Freeman and G. H. Lander (North-Holland, Amsterdam, 1984), Vol. 1, p. 415.

[43] V. A. Schmidt and S. A. Friedberg, Metamagnetism of $Ni(NO_3)_2 2H_2O$, Phys. Rev. B **1**, 2250 (1970).

[44] R. Birgeneau, G. Shirane, M. Blume, and W. C. Koehler, Tricritical-Point Phase-Diagram in $FeCl_2$, Phys. Rev. Lett. **33**, 1098 (1974).

[45] W. Knafo, D. Aoki, D. Vignolles, B. Vignolle, Y. Klein, C. Jaudet, A. Villaume, C. Proust, and J. Flouquet, High-field metamagnetism in the antiferromagnet $CeRh_2Si_2$, Phys. Rev. B **81**, 094403 (2010).

[46] P. Haen, F. Lapierre, P. Lejay, and J. Voiron, Susceptibility anisotropy in the $(Ce,La)Ru_2Si_2$ system, J. Magn. Magn. Mater. **116**, 108 (1992).

[47] A. V. Andreev, Y. Skourski, S. Yasin, S. Zherlitsyn, and J. Wosnitza, High-field magnetism and magnetoacoustics in uranium intermetallic antiferromagnets, J. Magn. Magn. Mater. **324**, 3413 (2012).

[48] R. Bidaux, P. Carrara, and B. Vivet, Antiferromagnetisme dans un champ magnetique I. Traitement de champ moleculaire, J. Phys. Chem. Solids **28**, 2453 (1967).

[49] H. D. Zhou, E. S. Choi, Y. J. Jo, L. Balicas, J. Lu, L. L. Lumata, R. R. Urbano, P. L. Kuhns, A. P. Reyes, J. S. Brooks, R. Stillwell, S. W. Tozer, C. R. Wiebe, J. Whalen, and T. Siegrist, Metamagnetic transition in single-crystal $Bi_4Cu_3V_2O_{14}$, Phys. Rev. B **82**, 054435 (2010).

[50] Y. Tokunaga, D. Aoki, H. Mayaffre, S. Krämer, M. H. Julien, C. Berthier, M. Horvatić, H. Sakai, T. Hattori, S. Kambe, and S. Araki, Interplay between quantum fluctuations and reentrant superconductivity with a highly enhanced upper critical field in URhGe, Phys. Rev. B **93**, 201112 (2016).

[51] A. Galatanu, Y. Haga, T. D. Matsuda, S. Ikeda, E. Yamamoto, D. Aoki, T. Takeuchi, and Y. Ōnuki, High-temperature magnetic investigations on uranium compounds, J. Phys. Soc. Jpn. **74**, 1582 (2005).